

Multiband oscillations emerge from a simple spiking network

Tianyi Wu^{1,2,*} · Yuhang Cai^{3,*} · Ruilin Zhang^{2,4} ·
Zhongyi Wang^{1,2} · Louis Tao^{2,5,†} · Zhuo-Cheng
Xiao^{6,†}

Received: date / Accepted: date / Edited: date

Abstract Collective cortical dynamics are well known to perform oscillations in multiple frequency bands simultaneously, such as alpha (8-12 Hz), beta (12.5-30 Hz), and gamma (30-120 Hz) bands, playing crucial functional roles in cortical information processing and animal behaviors. In the last few decades, numerous computational models have provided theoretical frameworks to understand the emergence of these oscillations from interaction of spiking neurons. However, due to the strong nonlinearity, the interplay between neuronal oscillations on multiple bands have rarely been investigated. In this paper, we demonstrate the emergence of multiband oscillations in a simple spiking network containing only one excitatory and one inhibitory population, while most of current studies claim the necessity of multiple inhibitory time scales (especially, multiple types of inhibitory neurons) to produce multiple bands. We offer a Poincaré section theory explaining the very robust bifurcations from single oscillatory band to multiple bands, which are located in the parameter space. In addition, we develop a couple of model reductions of the high dimensional, nonlinear, and stochastic spiking network model, which successfully capture the multibands dynamics and bifurcations. Furthermore, the reduced models reveal conserved geometrical features of bifurcations on the low-dimensional manifolds in the reduced state space. Our work provide a simple mechanism giving rise to multiband oscillations, hence....

Keywords Gamma oscillations · Synchrony · Homogeneity · Coarse-graining method

1 Author Summary

Author Summary PH

2 Introduction

3 Results

This paper investigates multiband neuronal oscillations by first illustrating the emergence of multiple frequency bands from the simulation of a simple spiking neuronal network. By classifying temporal dynamics with clusters of firing patterns (or multiple firing events), we propose a Poincare section theory which successfully explains how multiple frequency bands are formed by different numbers of

¹ School of Mathematical Sciences, Peking University, Beijing 100871, China;

² Center for Bioinformatics, National Laboratory of Protein Engineering and Plant Genetic Engineering, School of Life Sciences, Peking University, Beijing, 100871, China;

³ Department of Mathematics, University of California, Berkeley, CA, USA 94720;

⁴ Yuanpei College, Peking University, Beijing, 100871, China;

⁵ Center for Quantitative Biology, Peking University, Beijing, 100871, China;

⁶ Courant Institute of Mathematical Sciences, New York University, NY, USA 10003.

* These two authors contributed equally to this paper.

† Corresponding authors. L. Tao E-mail: taolt@mail.cbi.pku.edu.cn; Z.-C. Xiao E-mail: xiao.zc@nyu.edu

periods. Furthermore, a stochastic bifurcation analysis reveals that the multiband oscillation is prominent in the high dimensional parameter space. Based on the Poincare section theory, we also demonstrate that multiband oscillatory dynamics are well-captured by population level coarse-graining, and exhibit relatively conserved geometrical features in reduced phase spaces. Hence,

3.1 Multiband oscillations emerge from a small intergrate-and-fire network

3.2 Multibands arise from iterations of MFEs

3.2.1 MFE: A high-dimensional repeating dynamics

3.2.2 Stochastic bifurcation causing multiband oscillations

3.3 MFE dynamics captured by reduced models

4 Discussion

Methods

Integrate-and-Fire Network

Consider a N -neuron integrate-and-fire (IF) neuronal network with N_E excitatory neurons (E) and N_I inhibitory neurons (I), where the membrane potential (v_i) of each neuron is driven by a sum of synaptic currents:

$$\begin{aligned} \frac{dv_i}{dt} &= \left(g_i^{ext} + g_i^E \right) \cdot \left(V^E - v_i \right) + g_i^I \left(V^I - v_i \right), \\ g_i^{ext} &= S_i^{ext} \sum_{\mu_i^{ext}} G^E(t - t_{\mu_i^{ext}}), \\ g_i^E &= \sum_{\substack{j \in E \\ j \neq i}} S_{ij}^E \sum_{\mu_j^E} G^E(t - t_{\mu_j^E}), \quad g_i^I = \sum_{\substack{j \in I \\ j \neq i}} S_{ij}^I \sum_{\mu_j^I} G^I(t - t_{\mu_j^I}), \end{aligned} \quad (1)$$

where $g_i^{\{ext, E, I\}}$ stand for the external, excitatory and inhibitory conductances of neuron i . Each neuron receives excitatory spiking stimulus from an external source (μ_i^{ext}) and other excitatory/inhibitory neurons in the network $\mu_j^{\{E, I\}}$, where the strength of synaptic couplings are represented by S_i^{ext} and $S_{ij}^{\{E, I\}}$, respectively. A spike is released by neuron i when its membrane potential v_i reaches the threshold V^{th} . After this, neuron i immediately enters the refractory period, and remains there for a fixed time of τ^R before resetting to rest V^r . It is conventional in many previous studies to choose $V^{th} = 1$ and $V^r = 0$ [1]. Accordingly, $V^E = 14/3$ and $V^I = -2/3$ are the excitatory and inhibitory reversal potentials. Each spike changes the postsynaptic conductance with a Green's function,

$$\begin{aligned} G^E(t) &= \frac{1}{\tau^E} e^{-t/\tau^E} h(t), \\ G^I(t) &= \frac{1}{\tau^I} e^{-t/\tau^I} h(t), \end{aligned} \quad (2)$$

where $h(t)$ is the Heaviside function. The time constants, $\tau^{\{E, I\}}$, model the time scale of conductances of the excitatory and inhibitory synapses (such as AMPA and GABA [5]).

While Eq. (1) can model a network with arbitrary connectivity structure, in this paper, we focus on homogeneous networks. That is to say, whether certain spike released by a neuron of type Q is received by another neuron of type Q' is only determined by an independent coin flip with a probability $P_{Q'Q}$, where $Q, Q' \in \{E, I\}$. Furthermore, $S_{ij}^{\{E, I\}}$ are also considered as constants independent of i, j .

Three different levels of models are illustrated below. The *Markovian integrate-and-fire network* approximates Eq. (1) with a Markov process, and the following *reduced network* and *coarse-grained model* are reduced models of the Markovian full model.

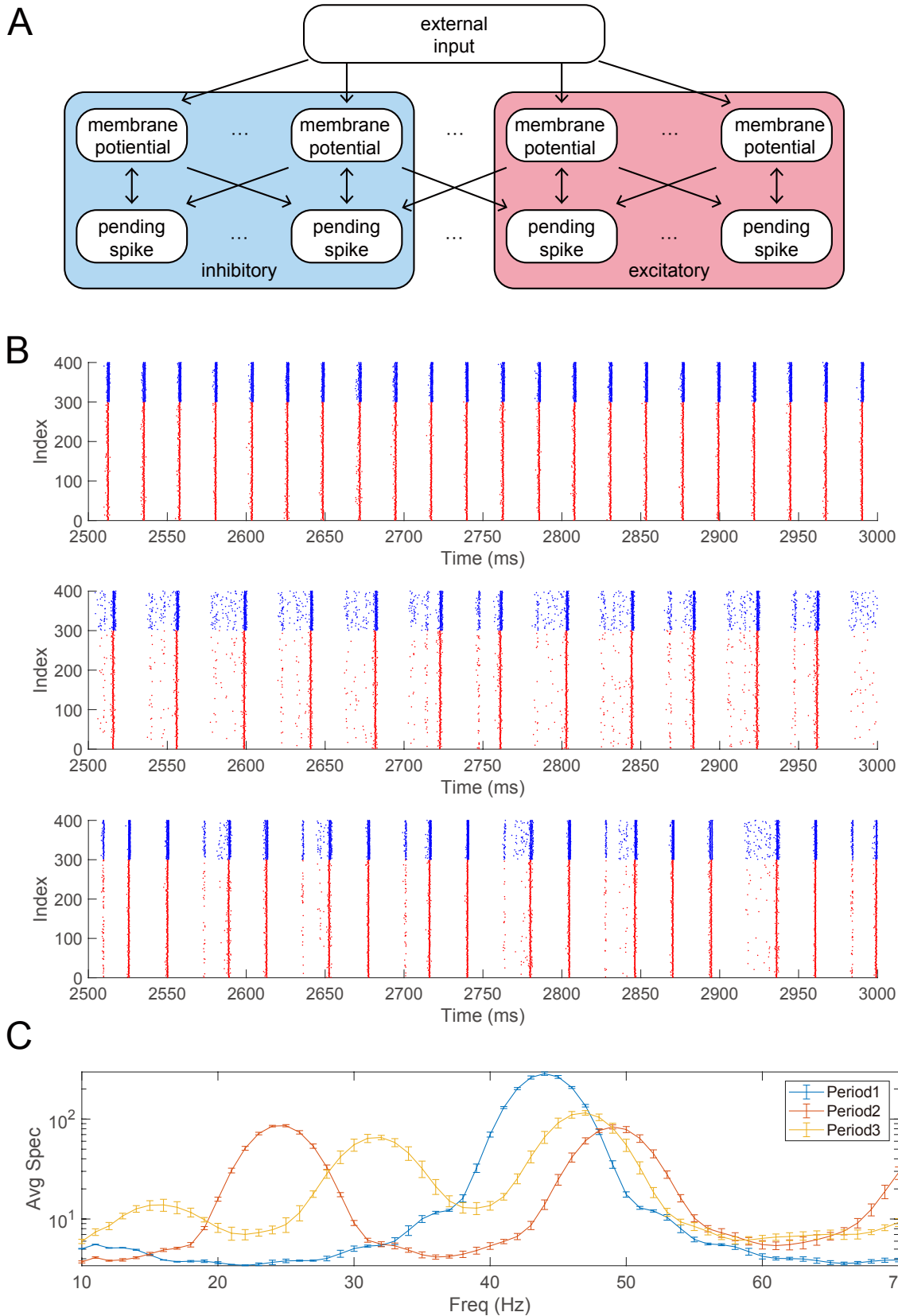


Fig. 1 Structures and important features of 3 models. **A.** The structure of the full Markovian integrate-and-fire network. **B.** The structure of the reduced network model, where the membrane potentials only take values in {Base, Gate}. **C.** The structure of coarse grained model. In this model the pending *E*-kick pools for every neuron are merged in to one for the whole network, and so are the pending *I*-kick pools.

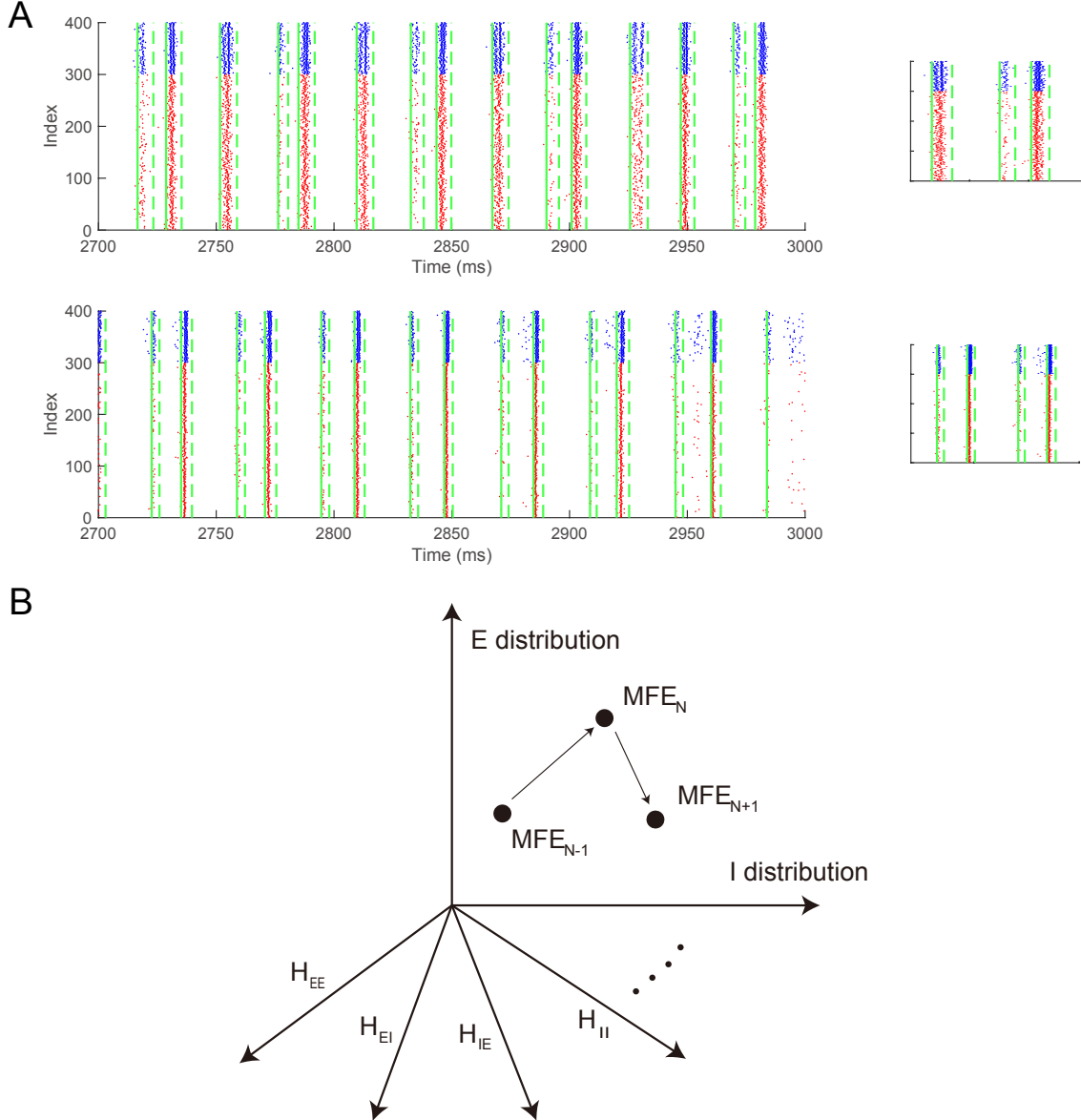


Fig. 2 Gamma oscillation exhibited by the MIF network in three different regimes. **A.** Homogeneous regime (“Hom”). Top: Raster plots of all 75 E -neurons (blue) and I -neurons (red) with firing rates noted in title. Middle: The spectrogram of the firing pattern exhibiting low density in the gamma band (30-80 Hz). Bottom: The spiking correlation diagrams for $\{E, I\}$ -spikes. **B and C.** Same as **A**. The regular (“Reg”) and synchronized (“Syn”) regimes exhibit much more synchronous firing patterns and stronger gamma-band activity.

Full Model: A Markovian Integrate-and-Fire Network

Following a previous study [6], we rewrite Eq. (1) as a Markov process to facilitate theoretical analysis. Therefore, we need to minimize the effects of the memory terms and discretize membrane potentials and conductances. Specifically, v_i takes values in

$$\Gamma := \{V^I, V^I + 1, \dots, V^r - 1, V^r, V^r + 1, \dots, V^{th}\} \cup \{\mathcal{R}\}, \quad (3)$$

To be consistent with the IF network, we choose $V^I = -66$, $V^r = 0$, and $V^{th} = 100$. As before, v_i enters the refractory state \mathcal{R} immediately after reaching V^{th} . However, in this Markovian IF (MIF)

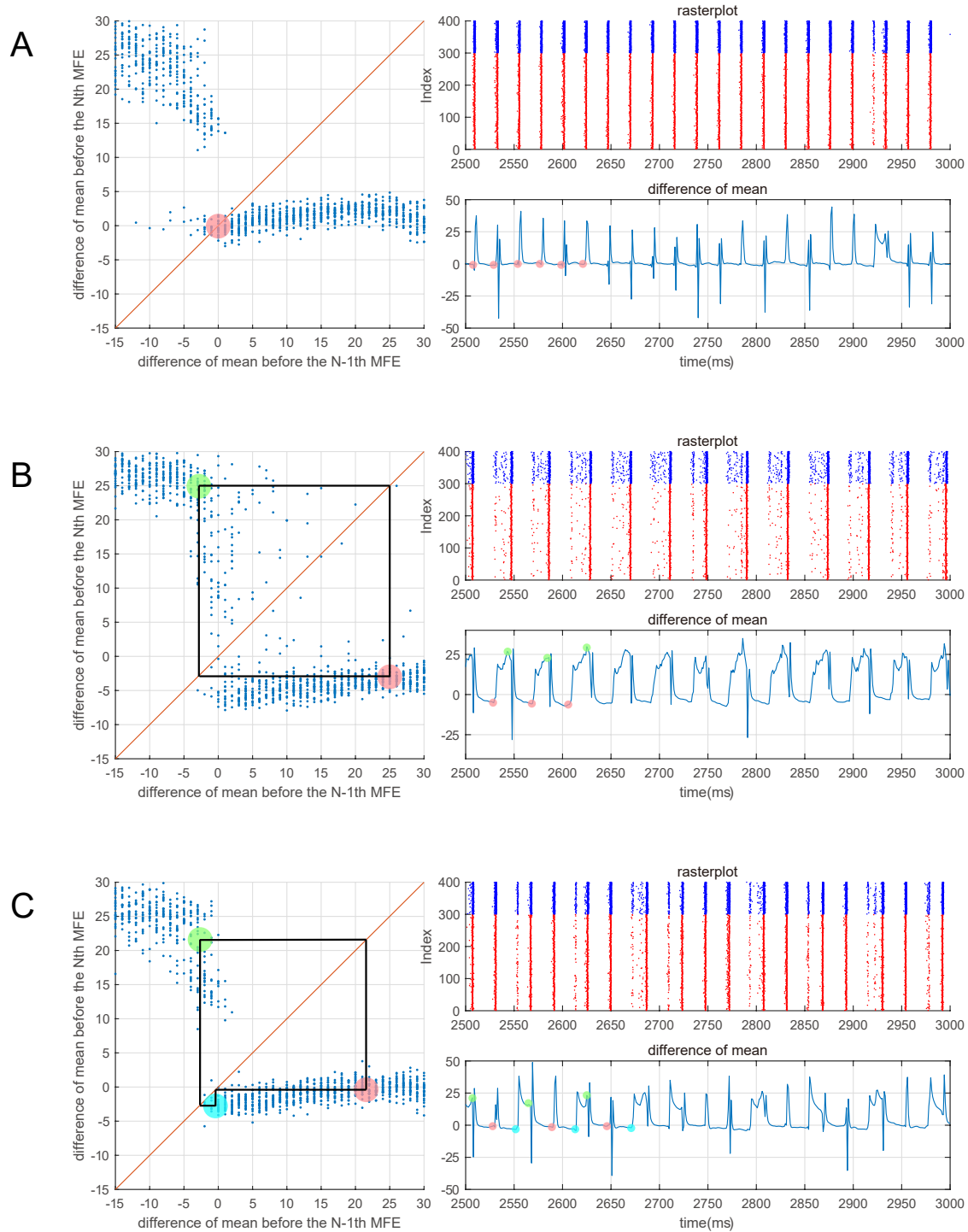


Fig. 3 Gamma oscillation captured by the reduced network consisting of two-state neurons. **A-C.** Same regimes and statistics investigated in Fig. 2.

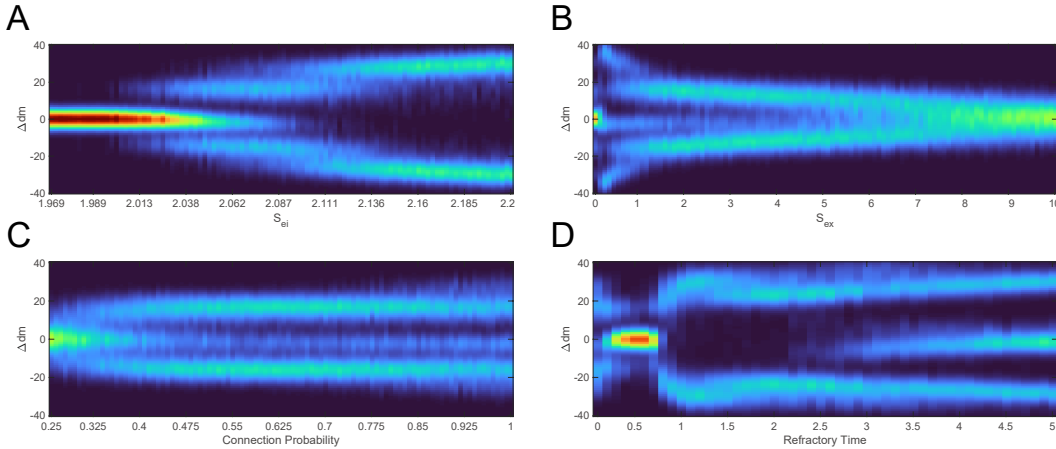


Fig. 4 Gamma oscillation captured by the coarse-grained model. **A-C.** Same regimes and statistics investigated in Fig. 1 and 2. The fake raster plots are produced by randomly assigning spikes to each neuron.

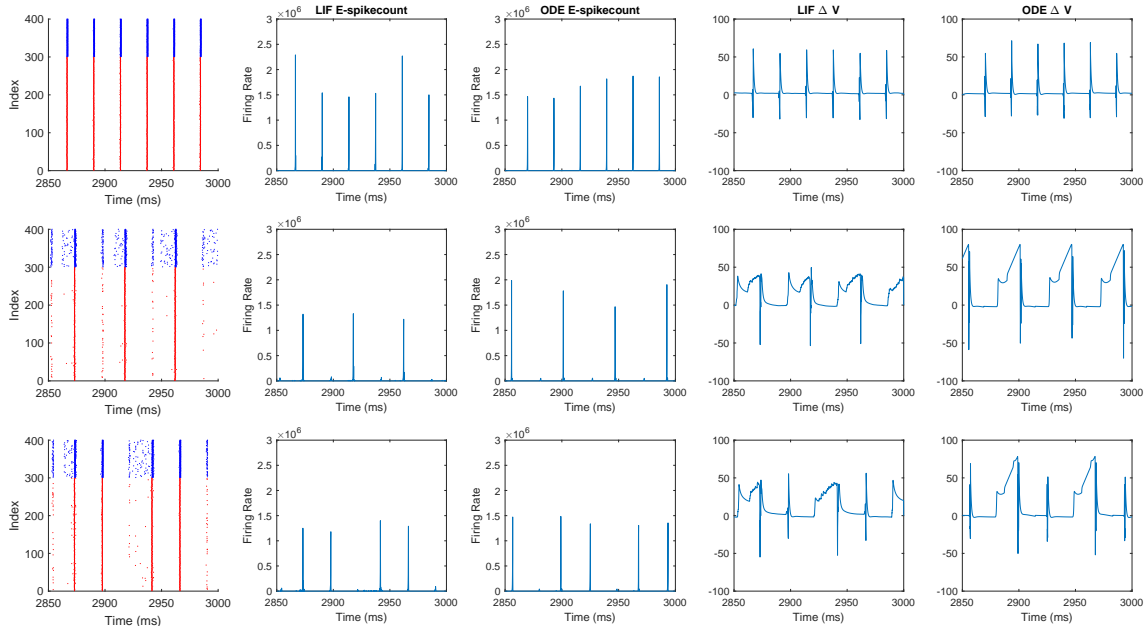
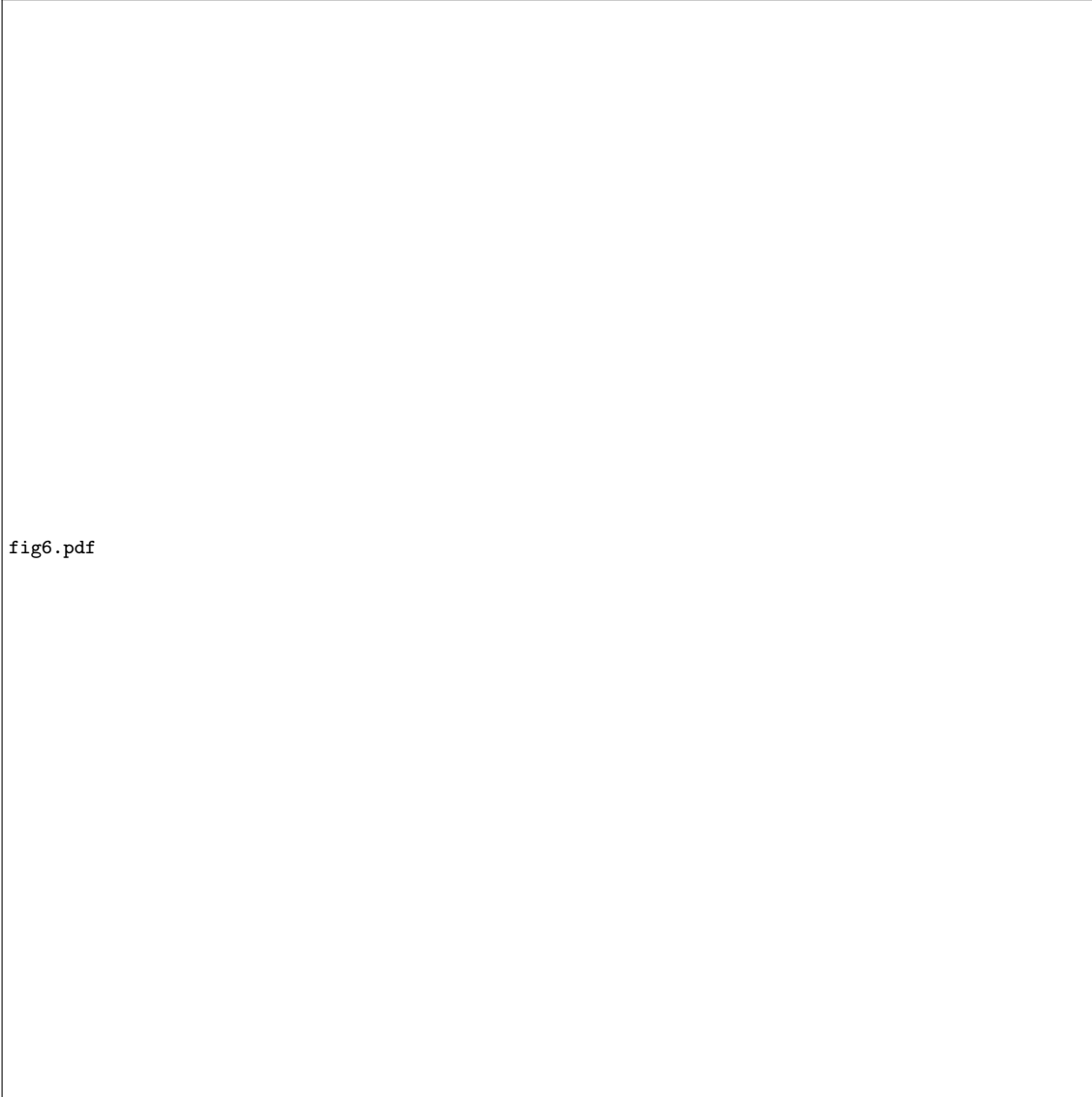


Fig. 5 Two gamma features captured by reduced models. **A.** MFE waiting time linearly related to external stimulation waiting time. Left: Syn regime; Right: Reg regime. **B.** Degree of synchrony decreases when τ^{EE} increases.

network, the total time spent in \mathcal{R} is no longer fixed, but an exponentially-distributed random variable $\tau^{\mathcal{R}}$.

Each neuron receives the external input as an independent Poisson process with rate $\lambda_{\{E,I\}}$, and v_i goes up for 1 when an external kick arrives. On the other hand, the synaptic conductances of each neuron $g_i^{\{E,I\}}$ are replaced by “pending-kick pools” $H_i^{\{E,I\}}$. Consider excitatory spikes for an example: Instead of updating g_i^E with Green’s functions when neuron i receives an E -spike, we add the new-coming spike to an existing spike pool H_i^E . Each spike in the pool will “take effect” to v_i independently (the precise meaning is explained below) after an exponentially-distributed waiting time τ^E , and H_i^E stands for the number of spikes has not taken effect yet. Therefore, for the a sequence of E -spikes received by neuron i , it is not hard to see that $\mathbb{E}[H_i^E(t)] = \mathbb{E}[g_i^E(t)]$.

**fig6.pdf****Fig. 6**

How each spike changes v_i is determined by the type of the spike (Q'), the type of neuron i (Q), and the state of v_i . When a spike takes effect, the membrane potential stays unchanged if $v_i = \mathcal{R}$, otherwise v_i may jumps up (for an E -spike) or down (for an I -spike). On the other hand, the size of the jump depends on the membrane potential, v_i , and the synaptic coupling strength, $S_{QQ'}$. For an E -spike, v_i should go up for S_{QE} . For an I -spike, however, the size of jump-down is $(v_i - V^I)/(V^{th} - V^I) \cdot S_{QI}$. The different arrangements here for $\{E, I\}$ -spikes are based on the following consideration: Due to the choices of reversal potentials, the currents induced by g_i^I is sensitive to v_i while the currents induced by g_i^E is not.

In our MIF network, we take most of the system (synaptic and stimulus) parameters directly from [6], but modified a few to accommodate the smaller network studied in this paper ($N = 100$, $N_E = 75$, $N_I = 25$). The parameters are summarized below:

- Frequencies of external input: $\lambda_E = \lambda_I = 7000$ Hz;
- Synaptic strength: $S_{EE} = S_{EI} = S_{II} = 20$, and $S_{IE} = 8$;
- Probability of spike projections: $P_{EE} = 0.15$, $P_{IE} = P_{EI} = 0.5$, and $P_{II} = 0.4$;

- Synaptic time-scales: $\tau^I = 4.5$ ms. $\tau^E < \tau^I$ to reflect the fact that AMPA is faster than GABA. We use different choices of τ^E for regimes implying different dynamics (all indicated in ms):
 1. Homogeneous (“Hom”): $\tau^{EE} = 4$, $\tau^{IE} = 1.2$,
 2. Regular (“Reg”): $\tau^{EE} = 1.7$, $\tau^{IE} = 1.2$,
 3. Synchronized (“Syn”): $\tau^{EE} = 1.4$, $\tau^{IE} = 1.2$,

Reduced Network Consisting of Two-State Neurons

The *reduced network* (RN) is a direct reduction of the MIF network by reducing the size of the state space for membrane potentials. In RN, each neuron i is a two-state neuron flipping between “base” or “gate” states, i.e., instead of taking values in the state space Γ , now $v_i \in \Gamma_2 = \{B, G\}$. A neuron in MIF network is deemed “base” or “gate” depending on how likely it is going to fire in the next couple of millisecond: Consider a certain cutoff $V^c \in \Gamma$, neuron i is a gate neuron if $v_i \geq V^c$ since it is closer to the threshold and is only a couple of E -kicks away from spiking. Otherwise, neuron i is a base neuron if $v_i < V^c$ or $v_i = \mathcal{R}$. Therefore, a flip from base to gate can take place when an E -spike or external stimuli takes effect and v_i crosses V^c from the lower side; on the other hand, a flip from gate to base may be due to v_i crossing V^c from the higher side when 1) an I -spike takes effect, or 2) the neuron fires and enters the refractory period.

The network with two-state neurons is reduced from the MIF network by combining states together, but generally we do not expect the full MIF model as a lumpable Markov process [13]. Therefore, the appropriate transition probability between the base and gate states should be carefully selected so that the RN can successfully capture the dynamics of the MIF network. Since the flip between states can only take place when certain kick takes effect, we list all possibilities as follows:

- **Effect of external stimuli:** When a kick arrives, a base $\{E, I\}$ neuron will become a gate $\{E, I\}$ neuron with probability $\{P_{ex}^{BE}, P_{ex}^{BI}\}$, while a gate $\{E, I\}$ neuron will fire and become a base $\{E, I\}$ neuron with probability $\{P_{ex}^{GE}, P_{ex}^{GI}\}$.
- **Effects of E-kicks:** Similar types of transitions here but different probabilities due to different sizes of kicks: $\{P_E^{GE}, P_E^{GI}, P_E^{BI}, P_E^{BE}\}$.
- **Effects of I-kicks:** The I-kicks do not have any effect on a base neuron. But I-kicks will depress a gate neuron to a base neuron with probabilities $\{P_I^{GE}, P_I^{GI}\}$.

All transition probabilities listed above are time-dependent and determined by the distribution of membrane potentials of neurons in the network, and we can collect their statistics from a long-time simulation of the MIF network. Here we illustrate how to compute P_E^{BE} for example, and everything else follows. Consider the distribution of membrane potentials of E -neurons, $p_E(v)$. Then P_E^{BE} is the conditional probability a base E -neuron goes across V^c within one E -kick, which is expressed as:

$$P_E^{BE} \{p_E\} = \frac{\int_{V^c - S_{BE}}^{V^c} p_E(v) dv}{\int_{v < V^c, v = \mathcal{R}} p_E(v) dv} \quad (4)$$

However, in RN, we do not see the exact distribution $p_E(v)$, but only the number of base and gate E -neurons (N_{GE}, N_{BE}) instead. Therefore, to set a closure condition for RN, we consider P_E^{BE} as a function of N_{BE} regardless of the specific distributions, i.e.,

$$\overline{P_E^{BE}}(N_{BE}) = E \left[P_E^{BE} \{p_E\} \mid \int_{v < V^c, v = \mathcal{R}} p_E(v) dv = \frac{N_{BE}}{N_E} \right] \quad (5)$$

Finally, to collect $\overline{P_E^{BE}}(N_{BE})$, we run the MIF network simulations for a long time and collect all the events when a E -kick takes effect and the membrane potential distribution satisfies the condition listed above. The estimate of $\overline{P_E^{BE}}(N_{BE})$ is hence the probability of one base E -neuron crossing V^c conditioned on these events.

Readers should note that, the three regimes (Hom, Reg, and Syn) investigated in this paper are only differentiated in the waiting time of kicks, i.e., the transition probabilities induced by single kicks are similar, given the observation that the subthreshold distributions in these regimes are alike. Therefore, to carry out reduction in these regimes, we only need the simulation of one canonical parameter set (say Syn) rather than all of them.

A Coarse-Grained Approximation

A *coarse-grained* (CG) approximation is developed to further reduce the number of states of the network. The MIF network has $O((168 \cdot n_H^2)^N)$ states, where n_H is the largest possible number of pending kicks for a neuron. The number for the RN is lower, as $O((2 \cdot n_H^2)^N)$, and yet it still grows exponentially with the size of the network. This number is already astronomical for the 100-neuron network studied in this paper.

A CG approximation of RN model is carried out as follows:

- First of all, due to the homogeneous connectivity of the network, all I -neurons have the same probability to add an E -kick to their pending-kick pools when an E -neuron i fires. Since each kick takes effect independently, this is equivalent to a large pool containing all E -kicks of the I -neurons and each E -kicks are randomly distributed to certain I -neuron when taking effect. Therefore, we only need the size of the large pool H^{IE} rather than looking into individual E -pending-kick pools for the I population. Likewise, we have pools H^{EE} , H^{EI} , and H^{IE} for other projections of spikes. Note that this CG simplification does not rule out autapses, i.e., the possibility that a spike takes effect on the neuron releasing it. This may be an issue when the network is very small; however, it does not cause any obvious problem in our model with 100 neurons.
- We now try to further combine the pools. Since all I -kicks are consumed with the same waiting time τ^I , we can combine the two I -kick pools together. This move does not directly apply to the two E -kick pools since $\tau^{EE} \neq \tau^{IE}$, and bias is introduced when we combine H^{EE} and H^{IE} , since they are consumed with different rates. We have to assume two constants $a^{EE} + a^{IE} = 1$ and

$$H^{EE} = a^{EE} \cdot H^E, \quad H^{IE} = a^{IE} \cdot H^E, \quad (6)$$

On the other hand, τ^{EE} and τ^{IE} are closer in the Syn regime, i.e., $H^{EE}/H^{IE} \approx \text{const}$ and the introduced bias is smaller in this regime (Fig. 7A). In all,

$$H^E = H^{EE} + H^{IE} = \sum_{i=1}^N H_i^E, \quad H^I = H^{EI} + H^{II} = \sum_{i=1}^N H_i^I, \quad (7)$$

where $H^{\{E,I\}}$ are the sizes of the $\{E, I\}$ -kick pools for the whole network.

- Finally, by definition, the transition probabilities of the two-state neurons are functions of the number of gate neurons (see Eq. 5). Therefore, instead of looking into the states of each neuron specifically, the distributions of membrane potentials are only determined by the numbers of gate neurons (N_{GE}, N_{GI}). Once they are determined, the number of base neurons come as

$$N_{GE} + N_{BE} = N_E, \quad N_{GI} + N_{BI} = N_I \quad (8)$$

Therefore, the CG approximation above is a Markov process with only four variables (N_{GE}, N_{GI}, H^E, H^I), and the number of states is $O(N^4) = N_E \cdot N_I \cdot (n_H)^2$. This is a tremendous reduction of scaling from exponential to polynomial in the size of the network. We here provide a qualitative description of the dynamics of the coarse-grained model: When an $\{E, I\}$ -kick takes effect, the number of $H^{\{E,I\}}$ minus one, and certain neuron flips between base/gate states with probability (represented by the change of N_{GE}, N_{GI}); If an $\{E, I\}$ -neuron fires, a spike is released and the pending-kick pool $H^{\{E,I\}}$ expands by

$$M_E = P_{EE}N_E + P_{IE}N_I, \quad M_I = P_{EI}N_E + P_{II}N_I, \quad (9)$$

where $M_{\{E,I\}}$ is the average number of postsynaptic neuron recipients of an $\{E, I\}$ -spike.

We list all possible transitions from state $X = (N_{GE}, N_{GI}, H^E, H^I)$ (Table 1). In addition, since all state transitions are triggered by certain kicks, which take effect independently with exponential waiting time, it is more important to know the the transition rates based on the transition probabilities. We list these rates in Table 2.

external kick takes effect	one E -kick takes effect	one I -kick takes effect
$N_{GE} + 1$	$N_{GE} + 1 \quad H^E - 1$	$N_{GE} - 1 \quad H^I - 1$
$N_{GI} + 1$	$N_{GI} + 1 \quad H^E - 1$	$N_{GI} - 1 \quad H^I - 1$
$N_{GE} - 1 \quad H^E + M_E$	$N_{GE} - 1 \quad H^E - 1 + M_E$	$H^I - 1$
$N_{GI} - 1 \quad H^I + S_I$	$N_{GI} - 1 \quad H^E - 1 \quad H^I + S_I$	
Remain	$H^E - 1$	

Table 1 All possible transitions from state $X = (N_{GE}, N_{GI}, H^E, H^I)$ to another. There are 13 cases in all.

external kick takes effect	one E -kick takes effect	one I -kick takes effect
$P_{ex}^{BE} N_{BE}/\lambda_E$	$P_E^{BE} a_{EE} \frac{N_{BE}}{N_E} H^E / \tau^{EE}$	$P_I^{GE} a_{EI} \frac{N_{GE}}{N_E} H^I / \tau^I$
$P_{ex}^{BI} N_{BI}/\lambda_I$	$P_E^{BI} a_{IE} \frac{N_{BI}}{N_I} H^E / \tau^{IE}$	$P_I^{GI} a_{II} \frac{N_{GI}}{N_I} H^I / \tau^I$
$P_{ex}^{GE} N_{GE}/\lambda_E$	$P_E^{GE} a_{EE} \frac{N_{GE}}{N_E} H^E / \tau^{EE}$	$(1 - P_I^{GE} a_{EI} \frac{N_{GE}}{N_E} - P_I^{GI} a_{II} \frac{N_{GI}}{N_I}) \cdot H^I / \tau^I$
$P_{ex}^{GI} N_{GI}/\lambda_I$	$P_E^{GI} a_{IE} \frac{N_{GI}}{N_I} H^E / \tau^{IE}$	
$(1 - P_{ex}^{BE}) N_{BE}/\lambda_E$ $+(1 - P_{ex}^{BI}) N_{BI}/\lambda_I$ $+(1 - P_{ex}^{GE}) N_{GE}/\lambda_E$ $+(1 - P_{ex}^{GI}) N_{GI}/\lambda_I$	$(1 - P_E^{BE}) a_{EE} \frac{N_{BE}}{N_E} H^E / \tau^{EE}$ $+(1 - P_E^{BI}) a_{IE} \frac{N_{BI}}{N_I} H^E / \tau^{IE}$ $+(1 - P_E^{GE}) a_{EE} \frac{N_{GE}}{N_E} H^E / \tau^{EE}$ $+(1 - P_E^{GI}) a_{IE} \frac{N_{GI}}{N_I} H^E / \tau^{IE}$	

Table 2 The transition rates of all transitions in Table 1.

Statistics

To quantify how well the reduced models (RN and CG) capture the dynamical features of the full model (MIF), we compare several statistics of the network dynamics (or more precisely, the spiking pattern produced by the network) collected from the simulations of the MIF, RN, and CG models. The reader should note that we can not tell the specific neuron indices of firing events in the CG model; yet it does not affect the computation of the statistics below. The raster plots produced for CG model, however, is indeed a mock-up raster plot by distributing spikes to neurons randomly among the appropriate ($\{E, I\}$) population.

Firing rates. Spikes from $\{E, I\}$ -cells are collected separately, and firing rates (fr_E, fr_I) are computed as the average numbers of spikes per neuron per second. All three models are simulated for over 3 seconds and spikes are collected from the 2nd second to rule out possible influences by the choice of initial conditions.

Spike synchrony index. We borrow the definition of spike synchrony index (SSI) from [2]. SSI describes the degree of synchrony of the firing events as the following. For each spike occurred at t , consider a w -ms time window centered by the spike $(t - w/2, t + w/2)$ and count the fraction of neurons in the whole network firing in such window. Finally, the SSI is the fraction averaged over all spikes.

It is not hard to see that SSI is larger for more synchronous spiking patterns. For the completely synchronized dynamics, every other neuron fires within the time window of each spike hence SSI=1. For completely uncorrelated firing patterns such as Poisson, SSI is a small number close to 0. One should note that the absolute value of SSI depends on the choice of the window size, and we choose $w = 5\text{ms}$ (the same as [2]).

Spectrogram. The power spectrum density (PSD) measures of the variance in a signal as a function of frequency. In this study, the PSD is computed as follows:

A time interval $(0, T)$ is divided into time bins $B_n = [(n-1)\Delta t, n\Delta t]$, $n = 1, 2, \dots$, the spike density μ_n per neuron in B_n is given by $\mu_n = m_n/N\Delta t$ where m_n is the total number of spikes fired in bin B_n . Hence, the discrete Fourier transform of $\{\mu_n\}$ on $(0, T)$ is given as:

$$\hat{\mu}(k) = \frac{1}{\sqrt{T}} \sum_{n=1}^{T/\Delta t} \mu_n \Delta t e^{-k \cdot (2\pi i) \cdot (n\Delta t)}. \quad (10)$$

Finally, as a function of k , PSD is the “power” concentrated at frequency k , i.e., $|\hat{\mu}(k)|^2$.

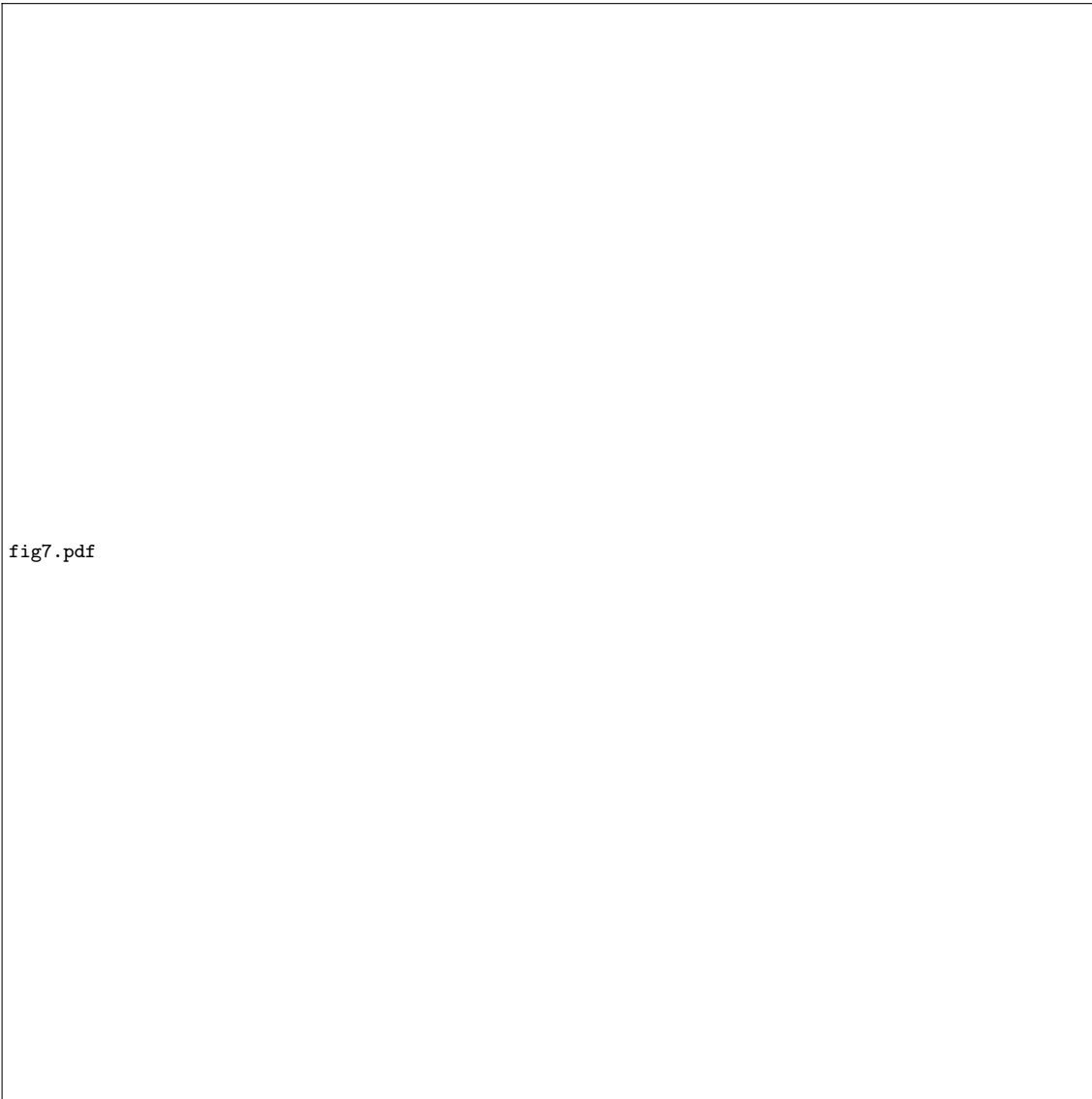


fig7.pdf

Fig. 7 Method Figure.

Spike timing correlations. The correlation diagrams describe the averaged correlation between each spike and others. Consider the correlation with I -spikes conditioned on E at $t = 0$:

For each E -spike at t , we take I -spikes within time window $[t - 15\text{ms}, t + 15\text{ms}]$, and compute the fraction of I -spikes in each 1-ms time bin. The correlation diagrams is then averaged over all E -spikes in this simulation.

Spiking volley detection. The method defining spiking volleys (or MFEs) is borrowed from [3]. The core idea of this method is to find time intervals with some length constraints that the firing rate of each time bin in this interval is a certain amount higher than the average firing rate. This is then defined as a spiking volley. We choose 1 ms time bin and $\delta = 0.33$, $\epsilon = 8$ as parameters (Fig. 7B).

Computational Methods

Exact timing of events. During our simulation, we can compute the exact timing of all events including firing, kicks taking effect, etc. We note that MIF, RN, and CG models are all Markov process

whose randomness mainly brought by the exponential distributions of various waiting times. Consider two independent events A and B with waiting time $X_A \sim \exp(\lambda_A)$, $X_B \sim \exp(\lambda_B)$, we have $\min\{X_A, X_B\} \sim \exp(\lambda_A + \lambda_B)$, i.e., the waiting time for either the first event is also an exponential distribution. Furthermore, the probability for the first occurring events to be A is $\lambda_A/(\lambda_A + \lambda_B)$.

Similar arguments extend to m events. By noticing that exponential distributed waiting times are temporally memoryless, we can simulated all three models by repeatedly selecting the first occurring event and generate the actual waiting time by sampling from certain exponential distributions.

Invariant probability distributions. After determining the total number of states and the transition probabilities between them, we can calculate the invariant probability distribution from the CG model by computing the eigenvectors and eigenvalues of the transition probability matrix. Such methods can be found in standard linear algebra textbooks such as [10].

Readers should note that theoretically, there is no upper bound for $\{H^E, H^I\}$. In order to close the computation of invariant probability distributions, we set the $n_{\{H^E, H^I\}}$, the largest numbers of pending spikes shown up in the simulations as the “boundaries” of the state space. Specifically, the transition probability from state X to Y is 0 if

1. $X = (N_{GE}, N_{GI}, n_{HE}, H^I)$ and $Y = (N_{GE}, N_{GI}, n_{HE} + a, H^I)$, or
2. $X = (N_{GE}, N_{GI}, H^E, n_{HI})$ and $Y = (N_{GE}, N_{GI}, H^E, n_{HI} + b)$,

where $a, b > 0$.

A “Shrunk” Coarse Grained Model. After the reductions, the CG model studied in this paper still has $M = 5.6 \times 10^9$ states. Though the first left eigenvector (i.e., the stationary probability distribution, corresponding to eigenvalue 1) of a sparse, M -by- M probability transition matrix is computable, the cost could be high for a desktop. Therefore, we aim at an even coarser version of the CG model: a “shrunk” coarse grained (SCG) model. Since $H^{\{E, I\}}$ are much higher than $N_{\{GE, GI\}}$, we shrink the CG model by combining every K states of pending kicks into one, i.e., all $1 \leq H_{CG}^E \leq K$ states in CG model is considered as $H_{SCG}^E = 1$ in SCG model. The intuition is the following: no need to characterize the states of pending spikes very precisely especially when the number is very large (i.e., the difference between 3000 and 3001 is very small). We choose $K = 24$ to keep it the same as S_{EE} .

Every state of SCG model can also be represented as a quadruplet $Q_{SCG} = (N_{GE}, N_{GI}, H_{SCG}^E, H_{SCG}^I)$. The SCG model works as follow. Firstly the quadruple Q_{SCG} is lifted to another quadruplet $Q_{CG} = (N_{GE}, N_{GI}, H_{CG}^E, H_{CG}^I)$, where $H_{CG}^{E,I} = (H_{SCG}^{E,I} - 0.5) \cdot K$. Then quadruplet Q_{CG} acts following the same rule as the CG model. Lastly the change of Q_{CG} is projected back into the change of Q_{SCG} :

1. The change of N_{GE} and N_{GI} in Q_{CG} is kept the same on corresponding elements in Q_{SCG} ;
2. The change x of $H_{CG}^{E,I}$ is replaced by change $y = [x/K] + b$ on $H_{SCG}^{E,I}$, where $[\cdot]$ denotes the least integer function and b is a Bernoulli variable with probability $p = (x/K) - y$;

Through this model, we can further reduce the M states of CG model to M/K^2 states of SCG model.

Locally-linear embedding. LLE is a nonlinear dimension reduction method which discovers the low-dimensional structure of high-dimensional data. More precisely, it maps the high-dimensional input data into a low-dimensional space. The core idea of LLE is to maintain the local linear structure through the mapping and this is achieved by a two-step optimization. There are N input data and we denote the high-dimensional input as \vec{X}_i and low-dimensional output as \vec{Y}_i . The algorithm is described below and more details see [11, 12].

1. Find the nearest k neighbors S_i^k of each data point \vec{X}_i ;
2. $W = \arg \min_{W'} \sum_i \|\vec{X}_i - \sum_j W'_{ij} \vec{X}_j\|^2$, $W'_{ij} = 0$ if $\vec{X}_j \notin S_i^k$;
3. $Y = \arg \min_{Y'} \sum_i \|\vec{Y}'_i - \sum_j W_{ij} \vec{Y}'_j\|^2$, subject to $\sum_i \vec{Y}'_i = 0$ and $\frac{1}{N} \sum_i \vec{Y}'_i \vec{Y}'_i^T = I$;

Dimensionality of data. We use local principal component analysis (local PCA) method to compute the local dimensionality of the data at each data point x , i.e., how its neighbors cluster around x . The data points processed here is selected from original data points with probability proportional to the square of distance from the place with highest density mass, in order to make the distribution of data points more uniform which can result in more precise local dimensionality characterization. For

x , consider the correlation matrix C_x of x and its K nearest neighbors (K selected as 100). Then the dimensionality at x is computed as

$$\text{Dim}(x) = \frac{\text{Tr}(C_x)^2}{\text{Tr}(C_x^2)} = \frac{(\sum_i \lambda_i)^2}{\sum_i \lambda_i^2} \quad (11)$$

where λ_i is the i -th eigenvalue of correlation matrix C_x . Eq. (11) is widely used as the dimensionality definition in theoretical and experimental neuroscience studies [4, 7–9].

Acknowledgments

This work was partially supported by the Natural Science Foundation of China through grants 31771147 (T.W., L.T.) and 91232715 (L.T.), by the Open Research Fund of the State Key Laboratory of Cognitive Neuroscience and Learning grant CNLZD1404 (T.W., L.T.). Z.X. is supported by the Swartz Foundation through the Swartz Postdoctoral Fellowship.

We thank Professors Yao Li (University of Massachusetts, Amherst), Kevin Lin (University Arizona), and Lai-Sang Young (New York University) for their useful comments.

References

1. Cai, D., Tao, L., Rangan, A. & McLaughlin, D. Kinetic theory for neuronal network dynamics. *Comm. Math. Sci.* **4**, 97–127 (2006).
2. Chariker, L., Shapley, R. & Young, L.-S. Rhythm and synchrony in a cortical network model. *Journal of Neuroscience* **38**, 8621–8634 (2018).
3. Chariker, L. & Young, L.-S. Emergent spike patterns in neuronal populations. *Journal of computational neuroscience* **38**, 203–220 (2015).
4. Gao, P. et al. A theory of multineuronal dimensionality, dynamics and measurement. *BioRxiv*, 214262 (2017).
5. Gerstner, W., Kistler, W. M., Naud, R. & Paninski, L. *Neuronal dynamics: From single neurons to networks and models of cognition* (Cambridge University Press, 2014).
6. Li, Y., Chariker, L. & Young, L.-S. How well do reduced models capture the dynamics in models of interacting neurons? *Journal of mathematical biology* **78**, 83–115 (2019).
7. Litwin-Kumar, A., Harris, K. D., Axel, R., Sompolinsky, H. & Abbott, L. Optimal degrees of synaptic connectivity. *Neuron* **93**, 1153–1164 (2017).
8. Mazzucato, L., Fontanini, A. & La Camera, G. Stimuli reduce the dimensionality of cortical activity. *Frontiers in systems neuroscience* **10**, 11 (2016).
9. Recanatesi, S., Ocker, G. K., Buice, M. A. & Shea-Brown, E. Dimensionality in recurrent spiking networks: global trends in activity and local origins in connectivity. *PLoS computational biology* **15**, e1006446 (2019).
10. Roman, S., Axler, S. & Gehring, F. *Advanced linear algebra* (Springer, 2005).
11. Roweis, S. T. & Saul, L. K. Nonlinear dimensionality reduction by locally linear embedding. *science* **290**, 2323–2326 (2000).
12. Saul, L. K. & Roweis, S. T. An introduction to locally linear embedding. *unpublished. Available at: <http://www.cs.toronto.edu/~roweis/lle/publications.html>* (2000).
13. Tian, J. P. & Kannan, D. Lumpability and commutativity of Markov processes. *Stochastic analysis and Applications* **24**, 685–702 (2006).

Supplementary Materials